Supplement Figure S1

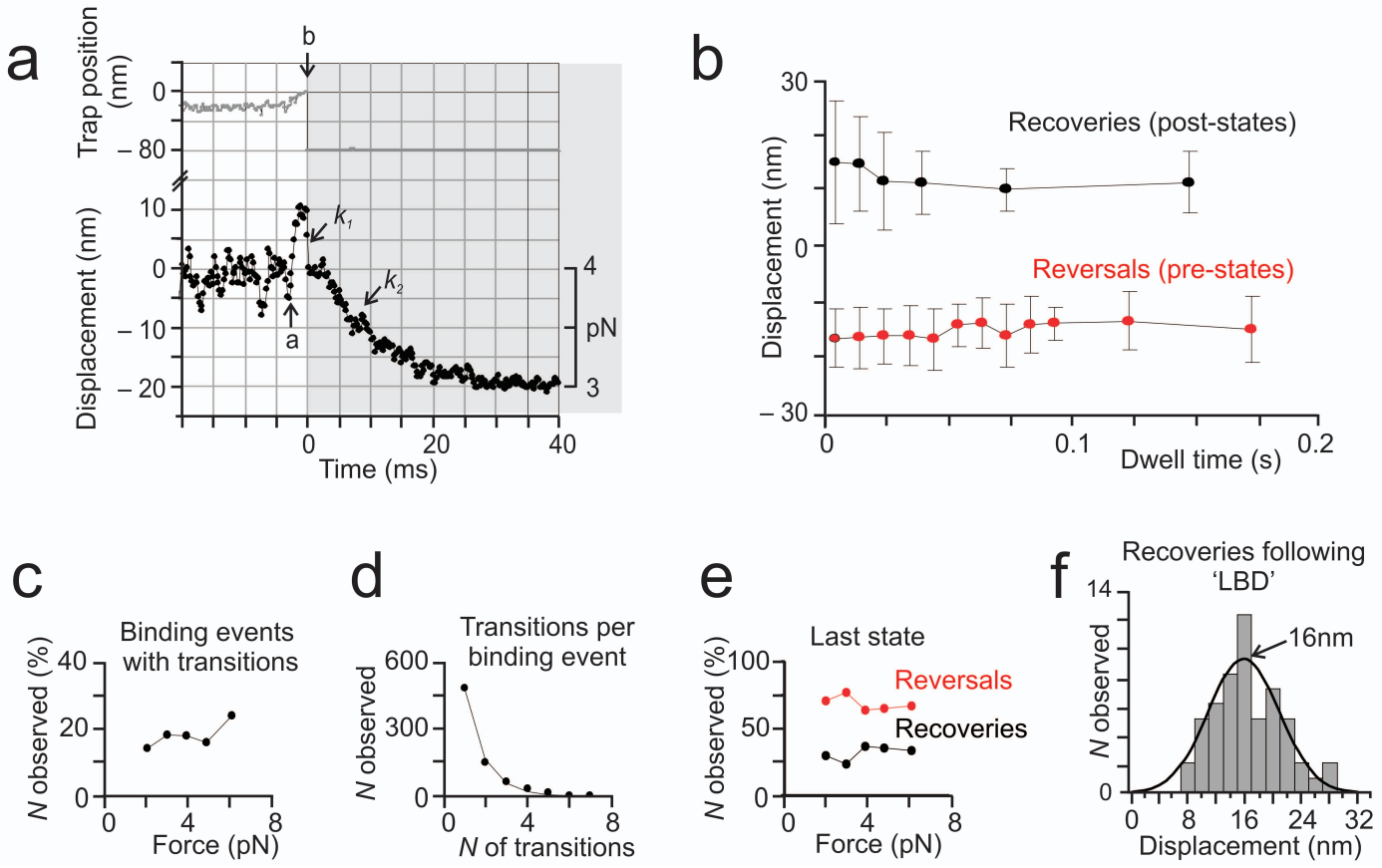

Nature Structural & Molecular Biology: doi:10.1038/nsmb.1820

FIGURE LEGEND

Supplementary Figure S1 Timing of load application and amplitudes of reversals and recoveries versus dwell times. **(a)** Ensemble average of 35 myosin binding events aligned towards the time point (b) when load was applied. Following on-line detection of myosin binding at time (a), load was applied within ~ 2 – 3 ms at (b), producing a fast series-elastic response (rate k_1). This is followed by a transition with a much slower rate constant (k_2) caused by myosin conformational change. **(b)** Amplitudes of reversals and recoveries, leading into pre- and post-states respectively, were binned according to the dwell time in the pre- and post-state respectively. Amplitudes are plotted as mean ± SD (*N* between 20 and 120 per bin). **(c)** Percentage of binding events that showed reversals (compared to the total number of binding events) at different loads. **(d)** The distribution shows the average number of transitions (reversals or recoveries) observed per binding event over the whole range of loads (2 – 7 pN). **(e)** The percentage of binding events that terminated on a reversal (red) or a recovery (black) is plotted against load. **(f)** The distribution of recovery strokes following large backward displacements ('LBD') could be fitted by a Gaussian (mean = 15.9 ± 5 nm, N = 17).

Supplement Figure S2

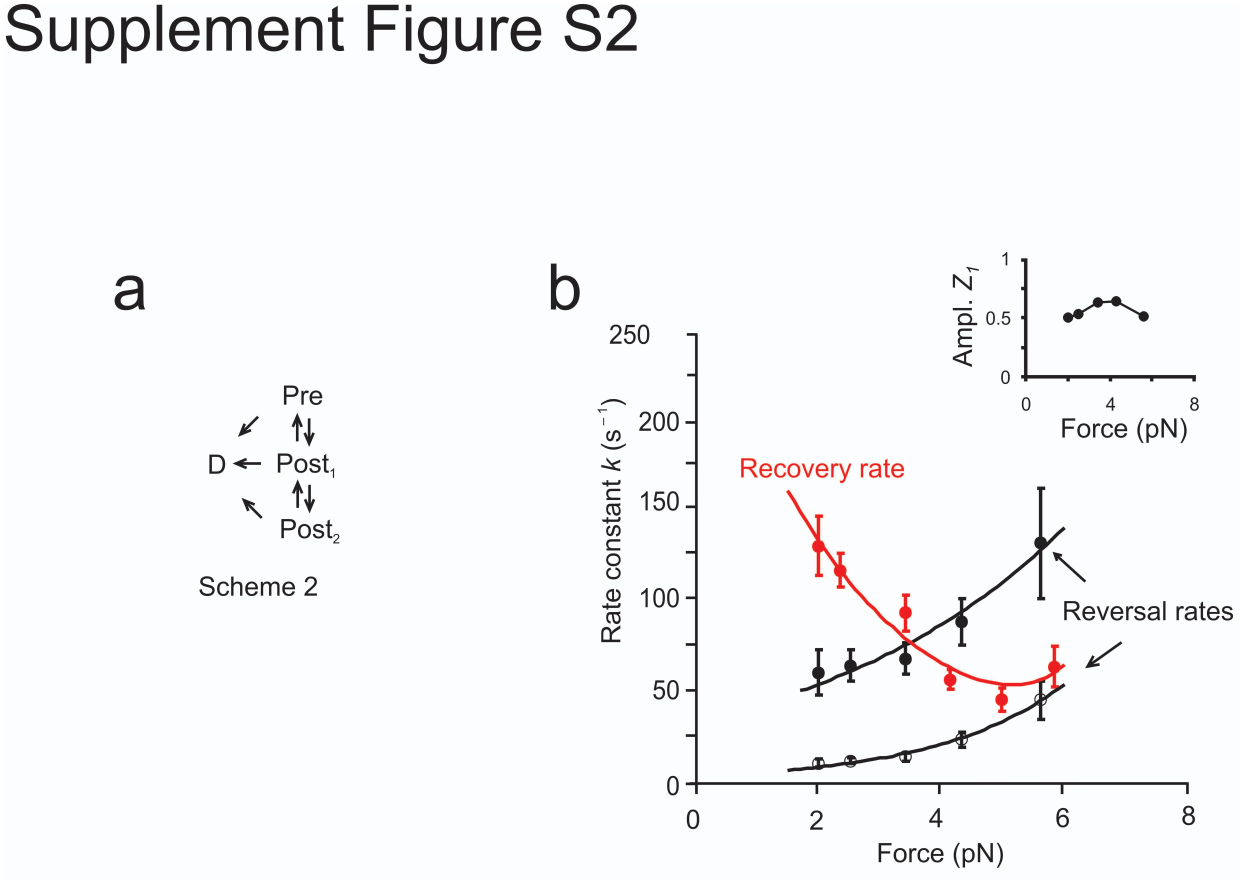

Nature Structural & Molecular Biology: doi:10.1038/nsmb.1820

FIGURE LEGEND

Supplementary Figure S2 Kinetics of pre- and post-states at different loads. **(a)** Scheme 2 shows transitions between one pre-power stroke state (pre), two post-power stroke states ($post_1$ and $post_2$) and detachment (D). The recovery and the two reversal rates were obtained by fitting the dwell-time distribution-plots (**Fig. 3,** main paper) of the pre-state by a single exponential, and those of the post-state by two exponential components, respectively. **(b)** The recovery rate (τ_{pre}^{-1}) and the two reversal rates ($\tau_{post\ 1}^{-1}$ and $\tau_{post\ 2}^{-1}$) are plotted against load. The inset shows the relative amplitude Z_1 of the faster reversal rate. The amplitude of the slower rate is ($1\text{-}Z_1$).

Supplement Figure S3

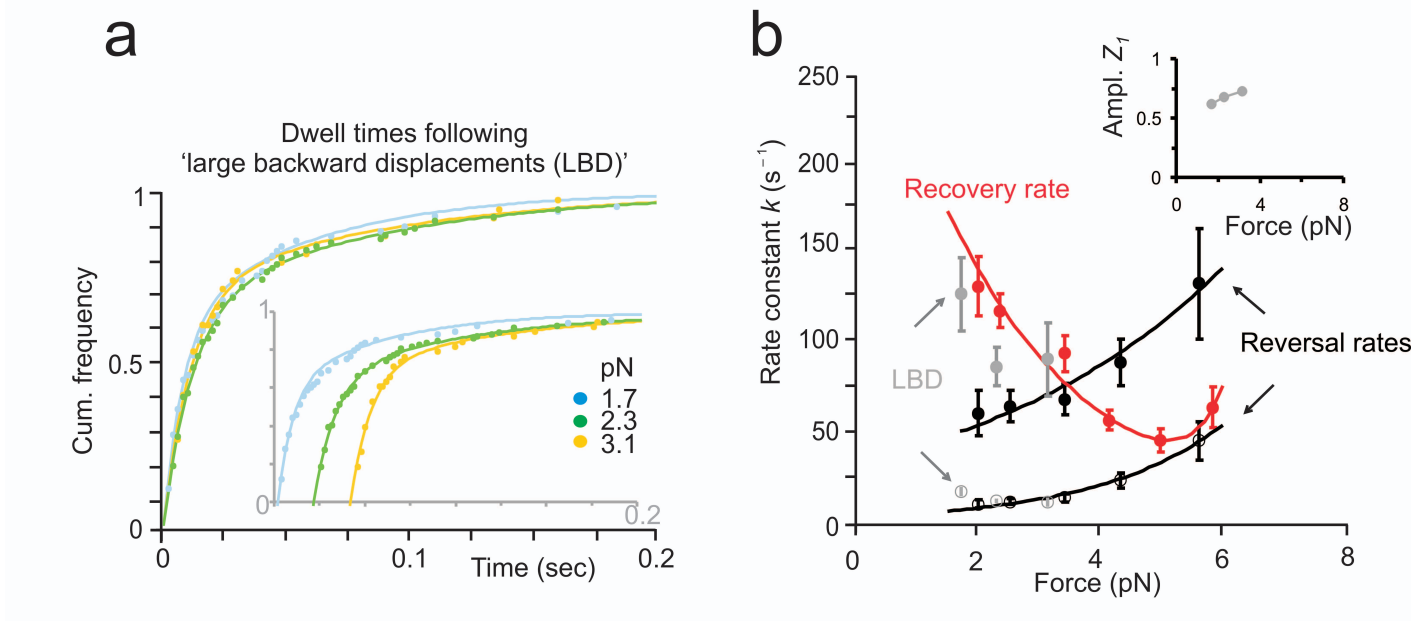

Nature Structural & Molecular Biology: doi:10.1038/nsmb.1820

FIGURE LEGEND

Supplementary Figure S3 Dwell times following large backward displacements (> 25 nm). **(a)** The cumulative distribution-plots of the dwell-times following large backward displacements (> 25 nm) were fitted by two exponential components (eq. 2). In the insets the plots were offset along the time axis for clarity. In **(b)** the rate constants of the fast and slow components are plotted against load (in grey). For comparison, the two reversal rates (in black) and the recovery rate (in red) are also shown. The inset shows the relative amplitude of the fast rate, Z_1, at different forces.

Supplement Figure S4

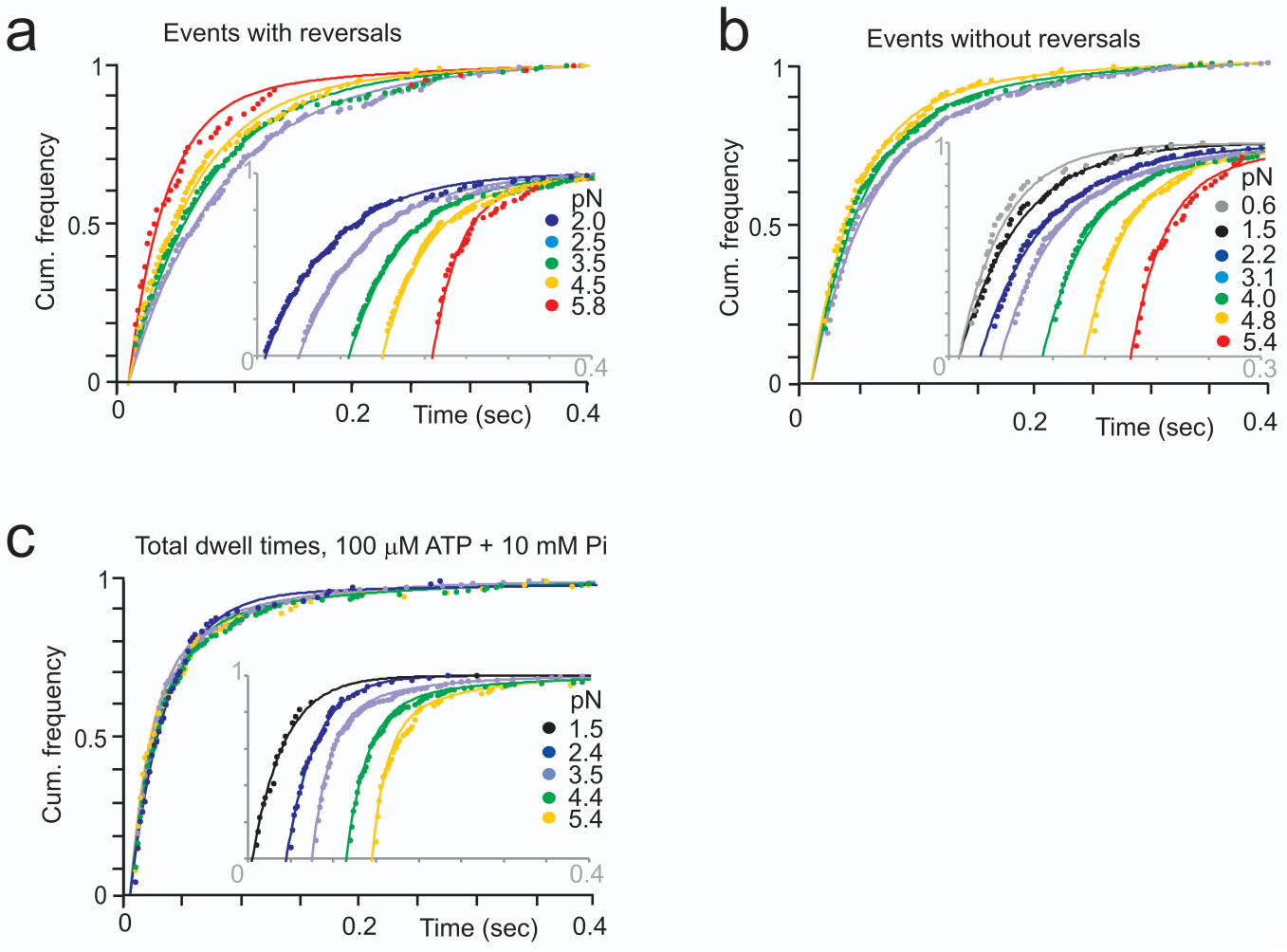

Nature Structural & Molecular Biology: doi:10.1038/nsmb.1820

FIGURE LEGEND

Supplementary Figure S4 Dwell times of binding events at different loads**. (a)** and **(b)** show cumulative distribution plots of the dwell times of myosin binding events. Dwell times of binding events for which reversals were resolved are plotted in **(a)**, those for binding events without reversals are plotted in **(b)**. The distribution plots at different loads were fitted by a single or two exponential components (**Supplementary Table 1)**. For clarity, the cumulative plots at different loads were offset along the time axis in the insets. **(c)** Cumulative distribution plots of dwell times of binding events, measured at 100 μM ATP in presence of 10 mM phosphate, were also described reasonably well by a single or two exponential components (**Supplementary Table 1**).

Supplement Figure S5

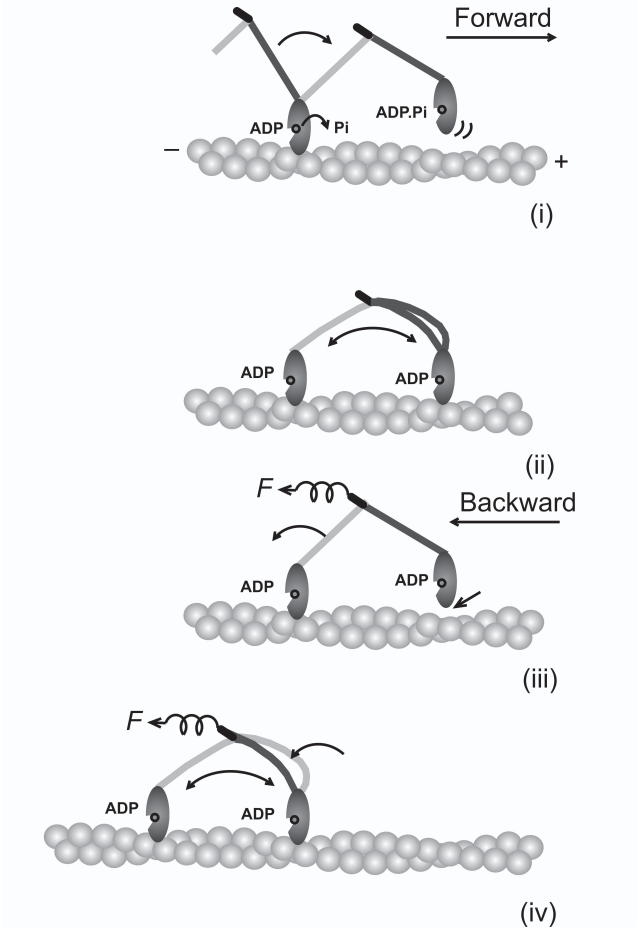

Nature Structural & Molecular Biology: doi:10.1038/nsmb.1820

FIGURE LEGEND

Supplementary Figure S5 Model for processive movement of dimeric myosin-Va. At low load, processive forward movement is achieved by a single bound head producing a power stroke towards the plus end of the actin filament (panel (i) and (ii)). At high loads, the lead head detaches (iii) and the power stroke of the remaining bound head is reversed (iv), facilitating processive backward movement.

Supplementary Table 1

	2.0 pN	2.4 pN	3.4 pN	4.2 pN	4.9 pN	5.6 pN	
Reversal (-5 to -25 nm) (N=259)	130±21 (40)	117±16 (54)	93±15 (49)	56±10 (32)	45±6 (53)	63±11 (31)	
	2.0 pN	2.5 pN	3.4 pN	4.3 pN	5.6 pN		
recovery (5 to 25 nm) (N=359)	k_1 60±13; k_2 10±2 Z_1 0.50 (45)	64±9; 11±2 0.53 (103)	68±9; 13±2 0.63 (97)	88±13; 23±5 0.64 (76)	131±31; 45±11 0.51 (38)		
	1.7 pN	2.3 pN	3.1 pN				
Large backward displacement (>-25 nm) (N=127)	k_1 125±20; k_2 17±3 Z_1 0.61 (39)	86±10; 12±1 0.68 (68)	90±20; 11±2 0.73 (20)				
	2.0 pN	2.5 pN	3.5 pN	4.5 pN	5.8 pN		
Total dwell time Events with reversals(N=567)	k_1 22±4 k_2 0.8±0.1 Z_1 0.68 (72)	13±1 0.9±0.1 0.7 (151)	16±1 1.6±0.1 0.73 (180)	19±2 4±0.4 0.75 (113)	35±5 5±0.7 0.9 (51)		
	0.6 pN	1.5 pN	2.2 pN	3.1 pN	4.0 pN	4.8 pN	5.4 pN
Events without reversals (N=1515)	22±4 (31)	12±2 (94)	k_1 18±1 k_2 4.1±0.4 Z_1 0.8 (308)	19±1 5.2±0.3 0.75 (460)	22±1 4.5±0.3 0.8 (377)	25±2 6.9±1.4 0.85 (184)	33±4 7.8±2.5 0.85 (61)
	1.5 pN	2.4 pN	3.5 pN	4.4 pN	5.4 pN		
Plus 10mM Pi (N=708)	27±5 (27)	29±3 (84)	k_1 49±3 k_2 9.5±0.7 Z_1 0.8 (254)	41±3 7.4±0.5 0.85 (264)	58±6 10.5±1.2 0.8 (79)		

FIGURE LEGEND

Supplementary Table 1 Rate constants ± SEM for dwell time distributions. Rate constants ± SEM determined from exponential fitting to dwell time distributions are summarised in this table. The unit for all rates is s^{-1}, the number of data included in each underlying fit is given in brackets. All experiments were carried out at 100 μM ATP and 29°C. For phosphate experiments 10 mM phosphate was included while the ionic strength of the solution was kept constant (~ 50 mM). For details of data analysis are given in the Methods section of the main paper.

Nature Structural & Molecular Biology: doi:10.1038/nsmb.1820

Direct observation of the myosin-V power stroke and its reversal

James R. Sellers and Claudia Veigel

SUPPLEMENTARY DISCUSSION

Protein preparations, solutions and optical trapping conditions

Baculo-virus expressed mouse myosin-Va fragment S1 (MVS1) was prepared as described [1]. This construct included the motor domain, neck region and all six light chain binding motifs. F-actin was polymerised using biotinylated G-actin (Cytoskeleton) at 30% of total actin and labelled with rhodamine phalloidin using standard methods [2]. Biotinylated polystyrene beads (1.1 μm diameter, Sigma) were suspended in 50 mM phosphate buffer pH 7.0 and incubated with 0.5 $mg.ml^{-1}$ Neutravidine (Pierce) for 20 min before being resuspended in phosphate buffer. The optical tweezers transducer built around a Zeiss Axiovert microscope has been described [1]. Flow cells were made from a microscope slide and pieces of coverslip. Glass beads (2.1μm diameter) were applied to the coverslip surface as a suspension in 0.1% w/v nitrocellulose/amyl acetate. MVS1 was bound unspecifically to the coverslip surface, using 10 – 50 $ng.ml^{-1}$ of protein in buffered salt solution (containing in mM: 25 KCl, 25 imidazole, 4 $MgCl_2$, 1 EGTA, pH 7.4, ionic strength ~ 50 mM). The experiments were carried out using this solution supplemented with (in mM); 2 creatine phosphate, 20 dithiothreitol, 0.01 – 0.1 ATP; and in $mg.ml^{-1}$; 1 creatine phosphokinase, 0.5 BSA, 3 glucose, 0.1 glucose oxidase, 0.02 catalase. ADP contamination was < 10 μM. Phosphate contamination (< 2 μM) was determined using phosphate binding protein [3]. For experiments in presence of 10 mM phosphate, the buffered salt solution contained (in mM): 4 $MgCl_2$, 10 KH_2PO_4 / K_2HPO_4, 1 EGTA, pH 7.4; ionic strength ~ 50 mM. In the experiments, a single actin filament (average filament length ≈ 4 μm) was attached at either end to a polystyrene bead (each held in an optical trap) and positioned close to a surface-attached glass bead.

Nature Structural & Molecular Biology: doi:10.1038/nsmb.1820

Interactions between actin and surface-bound myosin were monitored by casting the image of the trapped beads onto two quadrant-photodetectors [1]. The stiffness of a single optical trap κ_{trap} = 0.015 – 0.03 pNnm^{-1}. Data were sampled at 5 kHz. All experiments were carried out at 29^{o}C. Details on procedures to apply load and on data analysis are described in the main paper and below.

Mechanical response of the acto-myosin dumbbell to application of load

Supplementary Fig. S1a shows ensemble-averaged displacement data of 35 myosin binding events that were aligned using the time point (b) when load was applied. Myosin binding to actin and conformational change of ~ 10 nm occurred at time point (a) within our time resolution for detecting binding (~ 1 ms, see Methods), consistent with previous results [4]. With a time delay of ~ 2 – 3 ms following detection of binding, load was applied at time point (b). Both tweezers were moved in a stepwise fashion by a fixed distance parallel to the actin filament axis against the direction of myosin motion. Due to some spurious trap displacements during periods when myosin was not bound, the averaged trap position preceding myosin binding slightly deviates from resting position (= 0 nm). The ensemble- averaged mechanical response of the actin dumbell to the applied load consisted of two kinetic components; (i) a fast, transient displacement in direction of the applied load, consistent with a passive, series elastic component (rate k_1) and (ii) displacements on a slower time scale, probably due to conformational changes of the bound myosin (rate k_2). The time constant $2\pi (f_c)^{-1}$ of the series elastic response was determined by $f_c = \kappa_{total} (2\pi\beta)^{-1}$ with κ_{total} system stiffness and β viscous drag; $\kappa_{total} \sim 2\ \kappa_{trap} + \kappa_{add}$; single trap stiffness κ_{trap} = 0.015 – 0.03 pNnm^{-1}. Due to myosin binding κ_{add} increased from zero to ~ 0.2 pNnm^{-1}. The time constant for the series elastic response was ~ 0.5 ms. In order to separate the initial series elastic response from the displacements due to myosin conformational change we

Nature Structural & Molecular Biology: doi:10.1038/nsmb.1820

determined the bead position 2 ms after load was applied. This position was used as a reference point for subsequent changes in displacement in the data analysis.

Amplitudes of reversals and recoveries as a function of dwell times

We investigated whether there was a systematic change in amplitude of backward and forward displacements (i.e. 'reversals' and 'recoveries') with the dwell times of the pre- and post-power stroke states. **Supplementary Fig. S1b** shows that amplitudes of reversals and recoveries were both relatively broadly distributed, but independent of dwell time. In particular, there was no significant difference in amplitude between recoveries leading into short-lived or long-lived post-power stroke states. The kinetic analysis in **Fig. 3b**, main paper, suggested two populations of post-power stroke states, a short-lived and a long-lived one (**Supplementary Fig. S2b**). Thus the data are consistent with a model that involves two post-power stroke states in sequential order in the mechano-chemical cycle, that are linked by an isomerisation step without additional movement of the neck region of the motor. However, at present we can not exclude one of the two post-power stroke states to represent an off-pathway, only accessible under high load. It is also likely that the breadth of the distribution of amplitudes is added to by missed, short-lived reversals and recoveries (< 4 ms) that produced apparent intermediate levels of displacements. We will investigate this in further studies at higher time resolution.

Frequency of myosin binding events with reversals

Using a running *t*-test (see Methods) we identified statistically significant changes in displacement during myosin binding in ~20 – 30% of binding events at forces between 2 – 7 pN (**Supplementary Fig. S1c**). Up to 7 back and forth transitions per binding event were found at forces between 2 and 3 pN, while above 5 pN transitions were overwhelmingly backwards (**Fig. 2d,** main paper). The average number of transitions per binding event over the entire force range (2 – 7 pN) was ~ 1.6 (**Fig. 1b,** main paper and **Supplementary Fig. S1d**). The majority (60 –

Nature Structural & Molecular Biology: doi:10.1038/nsmb.1820

70%) of last transitions were reversal at all forces (**Fig. 1b**, main paper and **Supplementary Fig. S1e**), which explains that ~ 70% of all detected transitions were reversals (**Fig. 2b,** main paper). This suggests that the motor in pre-power stroke conformation is less strongly bound [5-7].

Reversal and recovery rates

As shown in **Fig. 3a,b** in the main paper, cumulative distribution plots of dwell times of the pre-state were described by single exponential functions. Two exponential components were required to describe dwell time distributions of the post-state, consistent with two post-power stroke conformations. **Supplementary Fig. S2a** shows a scheme for the transitions between two post-states, one pre-state and detachment. In this model, the two post-states do inter-convert. Because we have no further information at present about the nature of the two post-states, we simplified the scheme in the main paper. We lumped both states into one and calculated a single rate constant for the post-state at different loads (using eq. 3; Fig. 3c). In **Supplementary Fig. S2b** we plotted the reversal and recovery rates (characterising dwell times of the post-states and pre-state respectively; see **Fig. 3a,b**) at different loads. The inset shows the relative amplitude Z_1 of the faster reversal rate. Load dependence of the recovery rate was described by two exponential components (eq. 5), with $k_{01} = 284\ s^{-1}$; $d_1 = -1.5$ nm; $k_{02} = 0.03\ s^{-1}$; $d_2 = 4.6$ nm. This is consistent with at least two pathways out of the pre-state (i.e. possibly into post-state 1 and 2). Load dependence of the two reversal rates was described by single exponential functions (eq. 4) with $k_0 = 33\ s^{-1}$; $d = 0.9$ nm (fast component) and $k_0 = 2.9\ s^{-1}$; $d = 1.9$ nm (slow component).

Large backward displacements (> 25 nm)

We also characterised the dwell times of large backward displacements (> 25 nm) which, we suspected, were caused by fast detachment and reattachment (slippage) at high loads. The dwell-time distribution-plots in **Supplementary Fig. S3a** at different loads were fitted well by two exponential components (eq. 2). The load dependent two rates are similar to reversal and recovery

Nature Structural & Molecular Biology: doi:10.1038/nsmb.1820

rates. This is consistent with the model that the large backward displacements are a mixture of pre- and post-power stroke conformations (**Supplementary Fig. S3b**). This is expected if the large backward displacements were due to slippage along actin, with the crossbridge sometimes in pre- and sometimes in post-power stroke conformation. Slippage along the helical repeat of the actin filament could explain the population of ~ – 36 nm backward displacements, while a combination of slippage and power stroke reversal could cause those with – 46 nm mean amplitude. Consistent with this idea we also found 16 ± 5 nm recovery strokes following large backward displacements (**Supplementary Fig. S1f**).

Dominant state leading into detachment

We also investigated whether myosin would detach predominantly from a pre- or a post-power stroke conformation (**Supplementary Fig. S1e**). We found that the fraction of binding events detaching from a backward displacement was larger over the whole range of forces applied in this study, consistent with the pre-power stroke state less strongly bound to actin. However, we can not exclude that the 'reversals' at the end of binding events were partly caused by slippage along actin (see above). Thus, because the last backward displacements in a binding event are ill-defined we excluded them in the kinetic analysis of the population of reversals in this study and only included 'intermittent' reversals (< 25 nm) that were followed by a recovery.

Average dwell times of myosin bound to actin: comparison of events with and without reversals and the effect of added phosphate

We also compared the dwell times of binding events for which reversals were detected, with those for events without reversals (**Supplementary Fig. S4a,b**). Dwell-time distribution plots at different loads were all fitted reasonably well by either a single (eq. 1) or two exponential components (eq. 2) with the faster component (**Fig. 3c**, main paper) being dominant at all forces. All rates ± SEM are given in **Supplementary Table 1**. We found no difference between the two

Nature Structural & Molecular Biology: doi:10.1038/nsmb.1820

populations of binding events, consistent with the idea that the same process was rate limiting, i.e. a long-lived post-power stroke state at loads < 4 pN and a pre-power stroke state at loads > 4 pN (see **Supplementary Fig. S2**). In order to investigate the effect of phosphate on the dwell times of binding events we added 10 mM phosphate while keeping the ionic strength constant (see above). Dwell time distributions could be fitted by a single exponential (eq. 1) for forces < 3 pN and by two exponential components for larger forces (**Supplementary Fig. S4c** and **Table 1**). The detachment rates at different loads are shown and discussed in **Fig. 4b** in the main paper.

Model for processive forward and backward movement of dimeric myosin-Va

The observed effect of load on a single motor head in this study can help to explain the mechanical behaviour of processive movement of dimeric myosin-Va, as illustrated in **Supplementary Fig. S5**. At low load (< 2 pN) a single head binds in pre-power stroke conformation, releases phosphate and produces a 15 nm power stroke, which directs the free head forward, towards the plus end of the actin filament (i). Due to forward strain when both heads are bound, the lead head is held backwards in pre-power stroke conformation [8-10], until the trail head release ADP first, binds ATP and detaches from actin (ii). Backward strain on the remaining bound head is now released, which enables it to produce its power stroke, bringing the molecule back into state (i). At high loads (> 2 pN) the power stroke of the lead head is reversed (iii), facilitating detachment and processive backward movement (iv).

Nature Structural & Molecular Biology: doi:10.1038/nsmb.1820

REFERENCES

1. Veigel, C., Schmitz, S., Wang, F. & Sellers, J. R. Load-dependent kinetics of myosin-V can explain its high processivity. *Nat. Cell Biol.* **7**, 861-869 (2005).
2. Veigel, C., Bartoo, M. L., White, D. C. S., Sparrow, J. C. & Molloy, J. E. The stiffness of rabbit skeletal actomyosin cross-bridges determined with an optical tweezers transducer. *Biophys. J.* **75**, 1424-1438 (1998).
3. White, H. D., Belknap, B. & Webb, M. R. Kinetics of nucleoside triphosphate cleavage and phosphate release steps by associated rabbit skeletal actomyosin, measured using a novel fluorescent probe for phosphate. *Biochemistry* **36**, 11828-11836 (1997).
4. Veigel, C., Wang, F., Bartoo, M. L., Sellers, J. R. & Molloy, J. E. The gated gait of the processive molecular motor, myosin V. *Nat. Cell Biol.* **4**, 59-65 (2002).
5. De La Cruz, E. M., Wells, A. L., Rosenfeld, S. S., Ostap, E. M. & Sweeney, H. L. The kinetic mechanism of myosin V. *Proc. Natl. Acad. Sci. USA* **96**, 13726-13731 (1999).
6. Gebhardt, J. C. M., Clemen, A. E. M., Jaud, J. & Rief, M. Myosin-V is a mechanical ratchet. *Proc. Natl. Acad. Sci. USA* **103**, 8680-8685 (2006).
7. Rosenfeld, S. S. & Sweeney, H. L. A model of myosin V processivity. *J. Biol. Chem.* **279**, 40100-40111 (2004).
8. Burgess, S. *et al.* The prepower stroke conformation of myosin V. *J. Cell Biol.* **159**, 983-991 (2002).
9. Forkey, J. N., Quinlan, M. E., Shaw, M. A., Corrie, J. E. T. & Goldman, Y. E. Three-dimensional structural dynamics of myosin V by single-molecule fluorescence polarization. *Nature* **422**, 399-404 (2003).
10. Syed, S., Snyder, G. E., Franzini-Armstrong, C., Selvin, P. R. & Goldman, Y. E. Adaptability of myosin V studied by simultaneous detection of position and orientation. *EMBO J.* **25**, 1795-1803 (2006).